Received: 3 May 2022 | Accepted: 8 August 2022

DOI: 10.1111/1751-7915.14133

RESEARCH ARTICLE

microbial biotechnology Open Access

Engineering cell morphology by CRISPR interference in *Acinetobacter baylyi* ADP1

Jin Luo[1] | **Elena Efimova**[1] | **Daniel Christoph Volke**[2] | **Ville Santala**[1] | **Suvi Santala**[1]

[1]Faculty of Engineering and Natural Sciences, Tampere University, Tampere, Finland

[2]The Novo Nordisk Foundation Center for Biosustainability, Technical University of Denmark, Kgs. Lyngby, Denmark

Correspondence
Jin Luo, Faculty of Engineering and Natural Sciences, Hervanta Campus, Tampere University, Korkeakoulunkatu 8, Tampere 33720, Finland.
Email: jin.luo@tuni.fi

Funding information
Academy of Finland, Grant/Award Number: 310188 and 334822; Novo Nordisk Fonden, Grant/Award Number: NNF21OC0067758

Abstract

Microbial production of intracellular compounds can be engineered by redirecting the carbon flux towards products and increasing the cell size. Potential engineering strategies include exploiting clustered regularly interspaced short palindromic repeats interference (CRISPRi)-based tools for controlling gene expression. Here, we applied CRISPRi for engineering *Acinetobacter baylyi* ADP1, a model bacterium for synthesizing intracellular storage lipids, namely wax esters. We first established an inducible CRISPRi system for strain ADP1, which enables tightly controlled repression of target genes. We then targeted the glyoxylate shunt to redirect carbon flow towards wax esters. Second, we successfully employed CRISPRi for modifying cell morphology by repressing *ftsZ*, an essential gene required for cell division, in combination with targeted knock-outs to generate significantly enlarged filamentous or spherical cells respectively. The engineered cells sustained increased wax ester production metrics, demonstrating the potential of cell morphology engineering in the production of intracellular lipids.

INTRODUCTION

In microbial chemical production, synthesis pathways often compete with growth for carbon and cellular resources. While static modification, such as gene deletions, can have positive effects on production by redirecting carbon fluxes, they often perturb growth-related reactions and may thus lead to unwanted trade-offs in the overall process. Strategies involving dynamic regulation of pathway fluxes have been recently developed to alleviate the constraints related to the unbalanced distribution of resources (Brockman & Prather, 2015a; Hou et al., 2020; Wei et al., 2022). The dynamic control over gene expression can be achieved by a number of approaches, such as employment of transcriptional regulators or regulatory small RNAs (Brockman & Prather, 2015b). In our previous study, we developed an autonomous circuit that dynamically regulated the expression of isocitrate lyase, which allowed controlled distribution of carbon and energy between growth and lipid synthesis in *Acinetobacter baylyi* ADP1 (hereafter ADP1) (Santala et al., 2018).

In comparison with other targets for genetic engineering, cell morphology is often neglected but can also impact a bioprocess, particularly for the production of intracellular products (Jiang & Chen, 2016; Kozaeva et al., 2021; Volke & Nikel, 2018; Wang et al., 2019). For example, large-sized cells can provide more cellular

space to accumulate intracellular products, thus allowing for a higher product content (Jiang & Chen, 2016; Zhang et al., 2020). In addition, cell enlargement or aggregation has been suggested to be advantageous for downstream cell recovery processes through improved filtration efficiency and the use of convenient methods, such as sedimentation and press filtration, for cell recovery from fermentation broth (Wang et al., 2014, 2019; Yenkie et al., 2017).

The variables that affect cell size have been investigated in *Escherichia coli*, including mass doubling time, DNA replication initiation and DNA replication-cell division cycle (Si et al., 2017). Controlling cell division has been demonstrated as an effective strategy to engineer cell size for bioproduction (Jiang & Chen, 2016). In recent studies, cell enlargement has been achieved by down-regulation of *ftsZ*, an essential gene required for cell division, which was shown to improve the accumulation of polymers, such as poly(lactate-co-3-hydroxybutyrate) (PLH) and poly(3-hydroxybutyrate) (PHB) (Ding et al., 2020; Elhadi et al., 2016; Kozaeva et al., 2021). For example, Kozaeva et al. (2021) repressed the expression of *ftsZ* in a *Pseudomonas putida* strain engineered for enhanced PHB production, further increasing the PHB content from 28% (w/w) to 32% (w/w) and titre from 0.94 to 1.12 g/L in a batch culture. Ding et al. (2020) overexpressed a FtsZ inhibitor and downregulated a key enzyme for DNA synthesis in a *E. coli* strain engineered for PLH production, increasing the PLH content by ~100%. Besides cell size, manipulation of cell shape may also affect the capacity of cells for product accumulation; for example, spherical cells have a lower surface-area-to-volume ratio (SA/V) for unit volume than rod-shaped cells. For rod-shaped species, the rod shape is typically mediated by the 'rod complex', consisting of the actin homologue MreB and other proteins, including RodA (transglycosylase) and penicillin-binding proteins (PBP) (Carballido-López, 2019; Cho et al., 2016).

ADP1 represents an emerging model organism for research and engineering (Biggs et al., 2020; Cuff et al., 2012; Metzgar, 2004; Santala & Santala, 2021; Tumen-Velasquez et al., 2018). It not only shares most of the traits that make *E. coli* a convenient model organism but also possesses unique features, such as natural competence and genetic tractability (Metzgar, 2004). In addition, the bacterium is known for its ability to accumulate high-value storage compounds – wax esters (WEs) (Martin et al., 2021). We have previously engineered the WE production pathway by increasing the availability of the precursor acetyl-CoA and overexpression of the WE synthesis gene (Lehtinen et al., 2018; Luo et al., 2020; Santala et al., 2018). WE accumulation was also facilitated by employing a strategy that partitioned the carbon sources between growth and WE synthesis (Santala et al., 2021). However, cell morphology engineering has not been carried out for WE production. WEs are accumulated intracellularly, serving as the carbon and energy reservoir during nutrient starvation. The synthesis of WEs starts at the inner side of the cytoplasm membrane, forming membrane-bound lipid-prebodies, which are subsequently released to form matured lipid-bodies (Wältermann et al., 2005). It is yet to be explored how cell morphology changes affect WE body formation and whether the strategy can be applied with WEs.

A recent engineering strategy involves the clustered regularly interspaced short palindromic repeats (CRISPR) system (Qi et al., 2013). In nature, CRISPR is widely encoded by bacteria and archaea, providing protective mechanisms against the invasion of foreign genetic elements (Makarova et al., 2011). One of the most well-described CRISPR systems so far is from *Streptococcus pyogenes*, which relies on the single endonuclease Cas9. The CRISPR-Cas9 system provides RNA-guided site-specific DNA cleavage and has been repurposed as an efficient genome-editing tool (Jiang et al., 2013). Substitution of Cas9 for its catalytically inactive mutant, referred to as dCas9, which retains DNA-binding capacity but is unable to cleave DNA, can block RNA polymerases from transcription; this synthetic system is called CRISPR interference (CRISPRi) (Qi et al., 2013). An inducible CRISPRi system serves as a powerful tool for repression studies of essential genes and strain optimization by co-expression of *dCas9* with a single guide RNA (sgRNA) targeting specific genes (Guzzo et al., 2020; Woolston et al., 2018). CRISPRi can be used to target multiple loci at once, if more than one sgRNA is expressed. One of the simplest approaches to achieving this is the expression of a sgRNA transcript that is cleaved with an endonuclease (McCarty et al., 2020). For example, the endonuclease Cas6 (formerly known as Csy4) from *Pseudomonas aeruginosa* (Haurwitz et al., 2010) has been applied in different host strains for site-specific RNA processing (McCarty et al., 2019; Qi et al., 2012).

CRISPRi has been previously established and employed in ADP1 (Geng et al., 2019). The goal was to repress the expression of mobile elements, which was accomplished by placing *dCas9* and sgRNA under the control of constitutive promoters. Here, CRISPRi was further developed in ADP1 for metabolic engineering purposes, namely for the redirection of carbon flux and engineering of cell morphology that involves essential genes as targets. To allow conditional knockdowns, inducible systems for both *dCas9* and sgRNA were established and optimized. In addition, the ribonuclease Cas6 that allows simultaneous repression of multiple loci was studied to expand the CRISPR-based toolbox for ADP1. The developed systems were then investigated in the context of cell morphology and its effects on intracellular lipid (WE) production.

EXPERIMENTAL PROCEDURES

Strains and media

E. coli XL1-Blue (Stratagene, USA) was used as the host for cloning work. *A. baylyi* ADP1 (DSM 24193, DSMZ, Germany) was used for all the experiments. The details of all the strains used in the study can be found in Appendix S2.

Modified lysogeny broth (LB) media (10 g/L tryptone, 5 g/L yeast extract, and 1 g/L NaCl) supplemented with 0.4% (w/v) glucose were used to grow *E. coli* and ADP1 for cloning and strain construction. Modified LB media were also used in the experiments for characterization of CRISPRi and the cyclohexanone-controlled induction system, and cell size manipulation by *ftsZ* repression and piperacillin treatment; phosphate buffer (3.88 g/L K_2HPO_4 and 1.63 g/L NaH_2PO_4) and 0.4% (w/v) glucose were added in the media when double reporter – monomeric superfolder GFP and mScarlet – strains were used. Modified minimal media MA/9 were used to study *aceA* repression, and mineral salts media (MSM) were used in the experiments for WE production; the carbon sources, including casamino acids, acetate, glucose and oleic acid, were added as appropriate. The composition of modified MA/9 is 4.40 g/L Na_2HPO_4, 3.40 g/L KH_2PO_4, 1.00 g/L NH_4Cl, 0.008 g/L nitrilotriacetic acid, 1.00 g/L NaCl, 240.70 mg/L $MgSO_4$, 11.10 mg/L $CaCl_2$, 0.50 mg/L $FeCl_3$. The composition of MSM is 3.88 g/L K_2HPO_4, 1.63 g/L NaH_2PO_4, 2.00 g/L $(NH_4)_2SO_4$, 0.1 g/L $MgCl_2{\cdot}6H_2O$, 10 mg/L ethylenediaminetetraacetic acid (EDTA), 2 mg/L $ZnSO_4{\cdot}7H_2O$, 1 mg/L $CaCl_2{\cdot}2H_2O$, 5 mg/L $FeSO_4{\cdot}7H_2O$, 0.2 mg/L $Na_2MoO_4{\cdot}2H_2O$, 0.2 mg/L $CuSO_4{\cdot}5H_2O$, 0.4 mg/L $CoCl_2{\cdot}6H_2O$, and 1 mg/L $MnCl_2{\cdot}2H_2O$. Antibiotics were added when needed (15 μg/mL gentamycin, 25 μg/ml chloramphenicol, 50 μg/ml kanamycin and 50 μg/ml spectinomycin).

Genetic engineering

Molecular cloning was performed using established methods. Transformation and the homologous recombination-based genome editing of ADP1 were carried out as described previously (Santala, Efimova, Kivinen, et al., 2011). All the plasmids constructed, primers used in the study and the corresponding description can be found in Appendices S3 and S4. The sgRNAs used in the study are also included in Appendix S4.

The integration vector pJL1 for replacing ADP1's prophage site with *dCas9* was constructed by Gibson Assembly. For the construction, the plasmids pdCas9-bacteria (a gift from Stanley Qi, Addgene #44249) (Qi et al., 2013), pBAV1C-chn (Luo et al., 2019) and pIM1463 (a kind gift from Murin, Addgene #30505) (Murin et al., 2012) were used as templates for the amplification of *dCas9*, *chnR* and the cognate promoter P_{chnB}, and the backbone containing the sequences flanking the prophage site respectively. The plasmid pJL2 was derived from pJL1 by replacing the RBS for *dCas9*, BBa_0034, with BBa_J61138 using USER cloning. The integration vector pJL3 for the mScarlet gene integration at the prophage site was derived from pJL1 by replacing *dCas9* with the mScarlet gene by USER cloning. The plasmid pJL4 and pJL5 were derived from pJL3 by replacing the RBS BBa_0034 with BBa_J61138 and BBa_J61105, respectively, using USER cloning. The integration vector pJL6 for integration of *gfp* at the *poxB* (*ACIAD3381*) site was constructed by amplifying *gfp* from the plasmid pBG42 (Zobel et al., 2015) and cloning it to the vector pAK400c using restriction sites MunI and XhoI. The plasmid contains sequences flanking *poxB* (Santala, Efimova, Karp, et al., 2011) to facilitate genomic integration. The plasmid pJL7 differs from pJL6 in the way that it contains a kanamycin marker instead of a chloramphenicol marker and the sequences flanking *ACIAD3309* instead of *poxB*. The integration vector pJL9 for *acr1* (*ACIAD3383*) knock-out was constructed by cloning a chloramphenicol marker to the pUC57 plasmid containing the sequences flanking *acr1* (here named as pJL8, purchased from Genscript). The plasmid pJL10 was constructed by cloning the P_{T5}-*acr1*-kan^r cassette (Luo et al., 2020) to pJL8. The plasmid pJL11 contains a null sgRNA under the control of the arabinose inducible promoter, constructed by USER cloning: the plasmids pBAV1C-ara-luxCDE (Santala, Efimova, et al., 2014) was used to amplify the backbone as well as *araC* and the cognate promoter P_{araBAD}; the plasmids pSEVA238-CRISPR and pSEVA648 were used to amplify the sgRNA scaffold and the gentamycin resistance gene respectively. Other sgRNA expressing plasmids were derived from pJL11 by USER cloning. The specificity of sgRNAs was checked using Cas-OFFinder (Bae et al., 2014). The cassette containing the two-sgRNA array (targeting *gfp* and *mScarlet*) and the codon-optimized *cas6* were purchased from Genscript and further cloned to the sgRNA expressing backbone, resulting in pJL17. The plasmid pJL18 was derived from pJL17 by removing *cas6*. The sequences of the plasmids pJL1, pJL11, and pJL 17 can be found in Appendix S5.

The GFP reporter strain (ASA514, also contains the bacterial luciferase operon *luxCDABE* from *Photorhadus luminescens*) was constructed as described below: the strain ADP1 Δ*acr1*::kan^r/*tdk* (a kind gift from Veronique de Berardinis, Genoscope, France) was transformed with the plasmid pVKK81-T-lux described in Santala, Karp, et al. (2014) for genome integration of *luxCDABE*; the resulting strain was then transformed with pJL6 for integration of *gfp* at *poxB* site. The GFP and mScarlet double reporter strain

(ASA518) was constructed by transforming a *mScarlet* expressing strain (Losoi et al., 2019) with pJL7; the *gfp* and *mScarlet* genes are integrated at the sites of *ACIAD3309* and *poxB* respectively. Knock-out of the rod shape-determining genes, *mreB* and *pbpA*, was done by transformation with the linear cassettes constructed by assembling the corresponding left flanking sequence, a chloramphenicol marker, and the right flanking sequence using SOE-PCR.

Characterization of the cyclohexanone-controlled induction system

The strain ASA511 was used to characterize the cyclohexanone-inducible promoter system, which contains *mScarlet* (integrated into the genome) under the control of the cyclohexanone-inducible promoter. The strain was cultivated in modified LB media (5-ml/14-ml-cultivation tube) containing different concentrations of cyclohexanone at 30°C and 300 rpm. After 25 h, 200 μl of each sample was transferred to a 96-well plate (flat bottom, μClear™, white, Greiner) to measure mScarlet fluorescence and optical density at 600 nm (OD_{600}). The measurement was conducted in Spark multimode microplate reader (Tecan, Switzerland); the excitation and emission wavelength were set to 580 and 610 nm. The data of the induction experiment was fit to a model (see Supplemental Note in Appendix S1) using the lsqcurvefit function in MATLAB.

Fluorescence measurements for CRISPRi characterization

For the GPF reporter strains, cells were cultivated in 200 μl modified LB media in 96-well plates. The well-plate was incubated in Spark multimode microplate reader at 30°C; double orbital shaking was performed for 5 min twice an hour with an amplitude of 6 mm and a frequency of 54 rpm; OD_{600} and GFP fluorescence signal were measured every 30 min. The excitation and emission wavelength were set to 485 and 535 nm for GFP fluorescence measurement. For the GFP and mScarlet double reporter strains, cells were cultivated in 4 ml modified LB media in 14-ml-cultivation tubes, and phosphate buffer and 0.4% (w/v) glucose were also added to the media. The cultivation was conducted in a shaker at 30°C and 300 rpm. Samples were taken at 20 h for GFP fluorescence measurement. Due to the slow maturation of mScarlet, the samples were incubated at 4°C overnight before mScarlet fluorescence measurement. The expressions of *dCas9* and sgRNAs were induced at the beginning of the cultivation by adding 5 μM cyclohexanone and 1% (w/v) arabinose respectively.

Cultivations for repression studies and WE production

To study the repression of *aceA* by CRISPRi, cells were cultivated in 20 ml modified MA/9 media in 100-ml-flasks at 30°C and 300 rpm for 20 h; the media were supplemented with 0.2% (w/v) casamino acids and 40 mM acetate. Inducers were added at the beginning of the cultivation. For the *ftsZ* repression study, cells were cultivated in 5 ml modified LB media in 14-ml-cultivation tubes at 30°C and 300 rpm. Inducers were added when OD_{600} reached 0.2, after which the cultivation continued for 18 h. Induction was performed by adding 5 μM cyclohexanone and 1% (w/v) arabinose.

For WE production, cells were cultivated in 250-ml-flasks containing 50 ml MSM supplemented with 0.2% (w/v) casamino acids and different carbon sources. The cultivation was performed in three different conditions. In this first condition, 5 mM glucose and 60 mM acetate were added at the beginning and supplied twice at ~10 and ~21 h with a concentration of 5 and 60 mM respectively. The cultivation was performed for 34 h at 30°C and 300 rpm with an initial OD of 0.1. Inducers were added into parallel cultures when OD reached ~0.5 (early induction) and ~1.5 (late induction) respectively. In the second condition, 200 mM glucose was added, and cells were cultivated for 48 h at 25°C and 300 rpm. The initial OD was 0.1, and inducers were added into parallel cultures when OD reached ~1.5 (early induction) and ~4 (late induction) respectively. In the third condition, 10 mM glucose and 14 g/L oleic acid (65.0–88.0%, Sigma Aldrich) were supplemented. Cells were cultivated for 36 or 48 h at 30°C and 300 rpm with an initial OD of 0.05. After 12 h, 10 mM glucose was supplied. Induction was performed with 1% (w/v) arabinose and 50 μM cyclohexanone.

Analysis of cell size by microscopy

Cells were harvested by centrifugation at 5939 *g* for 10 min and resuspended and diluted with phosphate-buffered saline (PBS). The cell ODs after dilution ranged from 0.05 to 0.2. The cells (5–10 μl) were then heat-fixed on a microscope slide and stained with crystal violet staining reagent for 1 min and subsequently washed with tap water for several seconds. The cells were analysed under bright field illumination using Zeiss Axioskop 2 equipped with Achroplan 100× objective lens. Image processing and cell size analysis were done using the software Fiji-ImageJ (Schindelin et al., 2012). Briefly, images were processed through the following steps: 8-bit conversion, background subtraction, thresholding, hole filling (if needed) and particle analysis; any defect was manually removed. For each sample, 200–300 cells were taken randomly for

cell size analysis based on the cross-section areas using RStudio.

Cell sedimentation analysis

Cells were harvested by centrifugation at 5939 *g* for 5 min and resuspended with PBS in glass test tubes. All samples were diluted to an OD_{600} of 0.9 and left undisturbed at room temperature. The OD_{600} was measured periodically using the spectrophotometer Ultrospec 500pro (GE Healthcare Life Sciences).

Nile red staining

Nile red staining was applied to visualize neutral lipid bodies (Wältermann et al., 2005). Specifically, Nile red stock solution (0.5 mg/ml DMSO) was diluted to 0.5 μg/ml using PBS; cells cultivated with fatty acids were harvested by centrifugation at 13,362 *g* for 5 min. A higher centrifugation condition was used prior to Nile red staining compared to the microscopy analysis, because it was more difficult to separate cells from the medium when cells were cultivated with fatty acids. The cells were then resuspended with the diluted Nile red solution and incubated on ice for 30 min. After staining, cells were washed with PBS and used for visualization under the microscope with an appropriate filter.

Analysis of substrate consumption

Cell cultures were centrifuged at 13,362 *g* for 5 min, and the supernatant was collected and filtered with 0.2 μm pore size filters. The samples were further diluted with water and subjected to analysis with high-performance liquid chromatography (HPLC). The analysis was conducted with an LC-20 AC prominence liquid chromatograph (Shimadzu, USA) equipped with RID-10A refractive Index detector. Phenomenex Rezex RHM-monosaccharide H+ (8%) column (Phenomenex) was used, and 5 mM sulphuric acid was used as a mobile phase with a flow of 0.4 ml/min.

Analysis of WE production

WEs were visualized using thin-layer chromatography (TLC), as described before (Santala, Efimova, Kivinen, et al., 2011). Briefly, 1–3 ml of biomass was harvested from cultures by centrifugation. The cell pellets were resuspended in 500 μl methanol and vortexed for 30 min. Then, 250 μl chloroform was added, after which the samples were vortexed for 1 h. Then the samples were centrifuged again. Next, 250 μl chloroform was 250 μl PBS were added, and the samples were slowly swirled for 2 h. After that, centrifugation was applied, and the low phase was taken for TLC. Glass HPTLC Silica Gel 60 F_{254} plate (Merck) was used for TLC. The mobile phase was a mixture of hexane, diethyl ether, and acetic acid with a ratio of 90:15:1. Jojoba oil was used as the standard of WEs. The TLC plats were stained with iodine.

Quantification of WEs was carried out using ^{1}H nuclear magnetic resonance (NMR). The cells were harvested from 40 ml culture by centrifugation at 30,000 *g* for 30 min. The harvested cells were freeze-dried with Christ APLHA1-4 LD plus freeze dryer (Germany) for 24 h. The extraction of lipids from the freeze-dried cells and analysis with NMR were performed as described previously (Santala, Efimova, Karp, et al., 2011). The chemical shift of 4.05 ppm corresponds to the proton signal of α-alkoxy-methylene group of WEs. The integral value of the signal at 4.05 ppm was used to calculate the content of WEs. An average molar mass of 506 g/mol was used to calculate the WE titre in grams per litre (Lehtinen et al., 2018).

RESULTS

Establishment of inducible CRISPRi in *Acinetobacter baylyi* ADP1

To target growth-essential genes in ADP1, we first established an inducible CRISPRi system based on dCas9. To ensure tight control of the system, two induction systems were used to control the expression of *dCas9* and sgRNA separately (Figure 1A). An arabinose-inducible promoter was used to control the expression of sgRNA in a pBAV plasmid. The vector replicates in ADP1 with a medium copy number (~58 copies per cell) (Bryksin & Matsumura, 2010). The pBAV plasmid-based arabinose induction system was characterized in our previous study (Santala, Efimova, et al., 2014). A cyclohexanone-inducible promoter was optimized to control the expression of *dCas9* from the genome. For that, we used previously described genomic locus (the prophage site) as an integration site (Lehtinen et al., 2017; Murin et al., 2012) and the cyclohexanone induction system from the pBAV1C-chn plasmid (Luo et al., 2019) coupled with a red fluorescent gene (mScarlet) to study induction; 5 μM cyclohexanone was sufficient to fully induce the promoter, leading to very high fluorescence signals. The transfer function, showing the change in promoter activity in regards to cyclohexanone concentration, is given in Figure S1A, and the corresponding model for fitting the data is presented in Supplemental Note in Appendix S1. In addition, the constructed reporter strain showed >300-fold higher fluorescence signal than the background (Figure S1B), indicating some leakiness of the system.

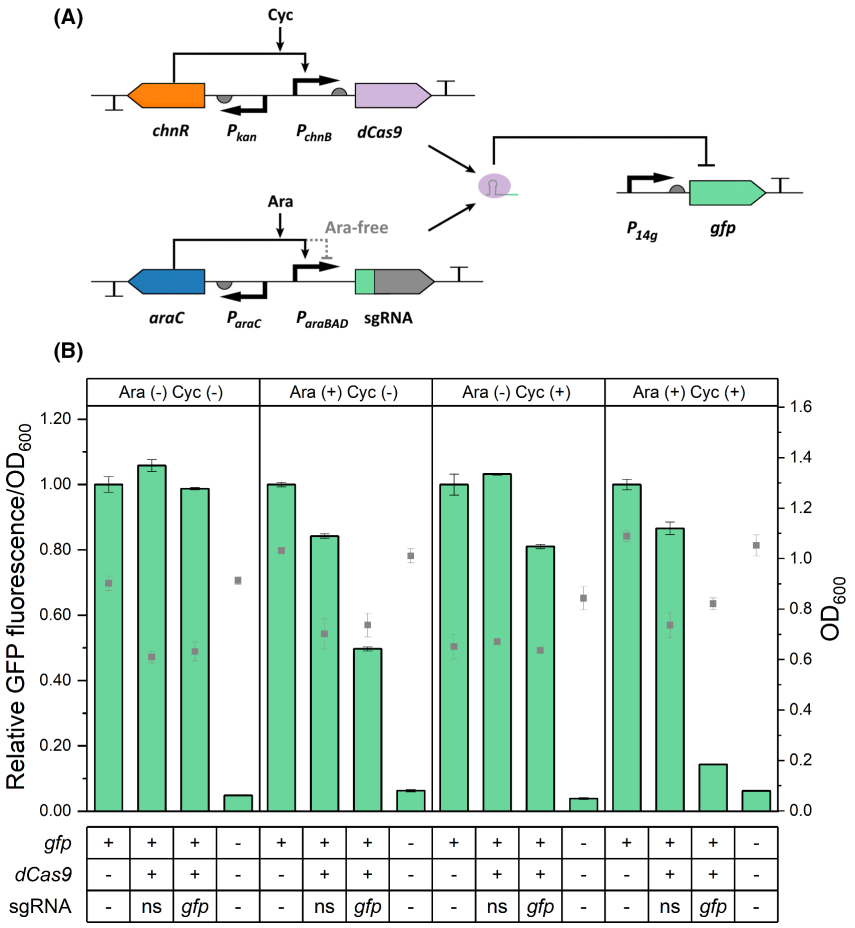

FIGURE 1 Characterization of the CRISPR interference system in *A. baylyi* ADP1. (A) Design of the CRISPRi system. The *chnR* regulator and *dCas9* are expressed from the genome, and the *araC* regulator and single guide RNA (sgRNA) are expressed from the pBAV plasmid. The *dCas9* gene and sgRNA (spacer sequence in green) are under the control of the cyclohexanone (Cyc)-inducible promoter and arabinose (Ara)-inducible promoter, respectively, while the *chnR* and *araC* regulators are constitutively expressed by the P_{kan} (promoter of the kanamycin resistance gene) and P_{araC} promoters respectively. ChnR and AraC act as activators when complexed with the corresponding inducers. The free AraC represses the P_{araBAD} promoter. The dCas9-sgRNA complex represses the expression of the *gfp* gene by targeting its coding sequence. (B) Analysis of the CRISPRi system under different induction states using GFP as the reporter. Cells were grown in LB media at 30°C in the presence (+) or absence (–) of arabinose (1% w/v) and cyclohexanone (5 μM). For each condition, the data at 26 h is shown as the fluorescence/OD_{600} relative to the values from the GFP reporter strain without sgRNA and *dCas9*. The time-dependent change of the fluorescence signal is presented in Figure S5. The table indicates either the presence (+) or the absence (–) of the genome-integrated *gfp*, *dCas9*, and the sgRNA-expressing plasmid. As controls, wild-type ADP1 and the GPF reporter strain containing *dCas9* and a non-specific (ns) sgRNA are used. The square symbols show the OD_{600} when the fluorescence measurement was performed. Data represent average values ± standard deviations of two independent biological experiments.

To evaluate the repression by the system, a reporter strain (ASA514) expressing the monomeric superfolder green fluorescent protein (hereafter GFP) was constructed. The strong constitutive promoter P_{14g} (Zobel et al., 2015) was used to drive *gfp* expression from the genome at the previously applied integration site (the *poxB* site) (Santala, Efimova, Karp, & et al., 2011). The CRISPRi machinery was then introduced into ASA514. In the initial experiment, a greatly reduced fluorescence signal was observed upon induction of the expressions of the *gfp*-targeting sgRNA (targeting base 41–60 of the coding region) and *dCas9* with 1% (w/v) arabinose and 0.2 μM cyclohexanone (Figure 1A; Figure S3). However, the full induction of *dCas9* with 5 μM cyclohexanone led to a notably decreased growth rate (Figure S4). We speculated that this is due to the toxicity of strongly expressed *dCas9*, presumably stemming from its non-specific binding to NGG sequences in the genome, particularly when unbound to a sgRNA (Zhang & Voigt, 2018). The dCas9-DNA complex that can interfere with DNA replication (Whinn et al., 2019) potentially burdens the cells. Although the levels of dCas9 can be reduced by lowering the inducer concentration, the low transcription and high translation rate would lead to high expression noise and in turn to phenotypic variation across the cell population and potentially raise uncertainties (Thattai & van Oudenaarden, 2001). As in the initial construct the expression of dCas9 was driven by the strong RBS (BBa_0034, iGEM Part Registry), we decided to tune its expression levels down. For

that, we further characterized two weaker RBSs (BBa_J61138 and BBa_J61105, iGEM Part Registry) in the cyclohexanone induction system for the expression of mScarlet gene. As expected, these RBSs lead to ~200 and ~2000-fold lower fluorescence intensities than BBa_0034 upon full induction (Figure S2).

Thus, the strong RBS (BBa_0034) preceding *dCas9* was replaced with the weaker RBS (BBa_J61138) to reduce the dCas9 dose when fully induced. Upon full induction, the strain with the weak RBS had a 3.3% reduction in growth rate, while the strain with the strong RBS exhibited a 32% reduction (Figure S4). The lower *dCas9* expression level still enabled effective gene repression; by inducing the expression of *dCas9* and the *gfp*-targeting sgRNA, the fluorescence of the strain decreased 86% (seven-fold decrease) compared to the reporter strain without the CRISPRi machinery (Figure 1B). Some background fluorescence signal was detected from the wild-type ADP1 without *gfp* (Figure 1B), most probably from media and cell components. Effective repression was maintained throughout the whole cultivation (Figure S5). Notably, some repression was also detected when only dCas9 or sgRNA expression was induced, indicating leakiness of both induction systems (Figure 1B). If neither of the systems was induced, no repression was observed. These results further emphasize the importance of using inducible promoters for both *dCas9* and sgRNA for a more tightly controlled system. It appears that the leakiness of the *dCas9* expression system is of particular concern, since induction of only *dCas9* expression led to a ~20% decrease in GFP fluorescence while a ~50% decrease was observed when only sgRNA expression was induced (Figure 1B).

Multiplex CRISPRi mediated by the ribonuclease Cas6

Motivated by the effectiveness of the single-guided CRISPRi, we set out to expand the system for multiplexed repression, by using a couple sgRNAs simultaneously. To this end, we employed Cas6 for processing a guide RNA array. Cas6 (formerly known as Csy4) is a ribonuclease of the CRISPR system in *P. aeruginosa* that processes primary CRISPR transcripts (Haurwitz et al., 2010). Two sgRNAs targeting *gfp* and *mScarlet* were combined in the guide RNA array (Figure 2A), which targeted base 41–60 and base 142–164 of the corresponding coding sequences respectively. The 20-bp Cas6 recognition sites (Figure S6) were placed upstream of each sgRNA and downstream of the second sgRNA. On the same pBAV plasmid, the *cas6* gene was expressed from the constitutive promoter BBa_J23150 (iGEM part). The two-sgRNA array was tested in a double reporter strain ASA518 containing *dCas9* under the transcriptional control of the cyclohexanone-inducible promoter. The *gfp* and *mScarlet* genes are integrated at the sites of *ACIAD3309* and *poxB* in the genome respectively, under the controls of the constitutive promoters P_{14g} and BBa_J23100 (iGEM part). As shown in Figure 2B, the GFP and mScarlet fluorescence was repressed by 69% and 61% respectively upon induction with 1% (w/v) arabinose and 5 μM cyclohexanone, indicating that the Cas6-mediated multiplex CRISPRi was well-functioning. A 20% reduction in GFP signal was observed for the control strain with the non-specific sgRNA upon induction (Figure 2B), which could result from high cellular burden due to co-expression of *mScarlet* and the CRISPRi machinery. Interestingly, in the control experiment, the strain lacking *cas6* also showed reduced GFP fluorescence upon induction but not for mScarlet (Figure 2B). It seems like the function of the first sgRNA in the unprocessed array, which targeted *gfp*, is neither affected by the 32 bases preceding the spacer (+1 site till spacer) nor by the succeeding second sgRNA (Figure S6). To further validate this, we tested the plasmid containing the guide RNA array but lacking *cas6* in the GFP single reporter strain; a clear reduction of fluorescence signal was observed upon induction (Figure S7). This result indicates that the guide RNA array may still be effective in guiding the repression of the gene targeted by the first sgRNA without the expression of *cas6*.

Applying the CRISPRi toolset for metabolic engineering

Modulating fluxes through the glyoxylate shunt by *aceA* repression

We next sought to demonstrate the use of the CRISPRi system for pathway modulation. The glyoxylate shunt replenishes the tricarboxylic acid (TCA) cycle intermediates from acetyl-CoA, bypassing the two oxidative steps that release two molecules of carbon dioxide (Figure 3A). The shunt is essential for the synthesis of the precursors required for growth when acetate is used as the sole carbon source. Isocitrate lyase, AceA, catalyses the first step of the glyoxylate shunt. Previously, it has been shown that in ADP1 gradual downregulation of *aceA* led to decreased biomass formation from acetate and redirection of the carbon flux towards fatty acid synthesis, thus enhancing WE accumulation (Santala et al., 2018). Here, we tested the repression of *aceA* by CRISPRi. We grew cells in MA/9 minimal media supplemented with casamino acids (0.2% w/v) and 40 mM acetate at 30°C. For induction, 1% (w/v) arabinose and 5 μM cyclohexanone were supplemented. With induction, WEs were detected after the 20 h of cultivation in the *aceA*-targeting strain, while WEs were not observed in the control strains (wild-type ADP1 and the *gfp*-targeting strain) (Figure 3B). The strain targeting *aceA* also showed slower growth and acetate consumption and

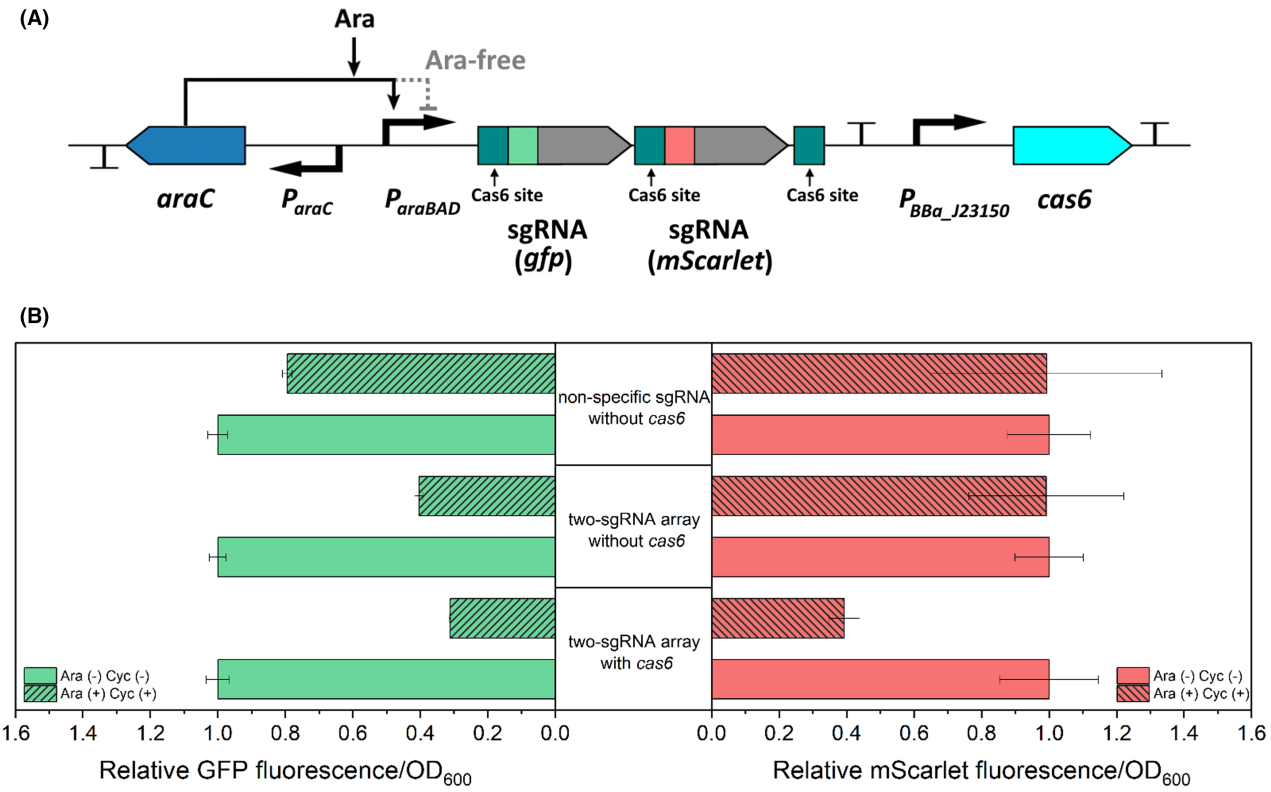

FIGURE 2 Characterization of the Cas6-mediated multiplex CRISPRi. (A) Design of the two-single guide RNA (sgRNA) array expressed in the pBAV plasmid. A Cas6 recognition site is placed before each sgRNA spacer sequence (in green and red). The third Cas6 recognition site is placed behind the second sgRNA. The expression of *cas6* is controlled by a constitutive promoter (iGEM part: BBa_J23150). (B) Simultaneous repression of *gfp* and *mScarlet* by the expression of the two-sgRNA array in the double reporter strain containing *dCas9*. Cells were grown in buffered LB containing 0.4% (w/v) glucose and cultivated at 30°C. Samples were taken for fluorescence measurement after 20 h of cultivation. The fluorescence values for each strain were normalized to the values measured for this strain without being induced by cyclohexanone (Cyc) and arabinose (Ara). Two *cas6*-negative strains were used as the controls, which carried the two-sgRNA array and a non-specific sgRNA respectively. Data represent average values ± standard deviations of two independent biological experiments.

a lower final optical density at 600 nm (OD_{600}) upon induction compared to the control strains (Figure 3C), indicating effective repression of the glyoxylate shunt for acetate metabolism. In the absence of inducers, there was no significant difference in specific growth rates (Student's *t*-test; *p*-value = 0.695) and average acetate consumption rates (Student's *t*-test; *p*-value = 0.963) between the two CRISPRi strains targeting either *aceA* or *gfp* (Figure 3D); wild-type ADP1 showed slightly faster growth and acetate consumption than the strains containing the CRISPRi system (Figure 3D). The successful redirection of the carbon flux to WE synthesis demonstrates the CRISPRi as an effective tool for pathway modulation.

Manipulating cell morphology by *ftsZ* repression

Cells with large size and/or atypical morphology can have benefits for intracellular product accumulation and downstream processing, such as higher storage capacity and easier cell harvesting (Jiang & Chen, 2016; Wang et al., 2019). Cell division is one of the processes that can be manipulated to control cell size: a shortened division period decreases cell size, and a prolonged division period leads to cell elongation. To realize cell enlargement in APD1, we applied the CRISPRi system to repress *ftsZ*, one of the essential genes for cell division (Figure 4A). We also sought to test the effect of *ftsZ* repression in the context of both rod-shaped and spherical (rod system negative) strains to determine if the SA/V differences impact WE accumulation (Figure 4A).

We first validated the strategy by treating a rod-shaped strain and two spherical strains (deletions of *mreB* or *pbpA*) with piperacillin. Piperacillin is a penicillin beta-lactam antibiotic that inhibits PBP3, a central component of cell divisome (Kocaoglu & Carlson, 2015). Thus, piperacillin treatment may have a similar effect as *ftsZ* repression. As expected, after piperacillin treatment, cell filamentation was observed for the rod-shaped strain, and large spherical morphology was observed for the *mreB* and *pbpA* mutants (Figure S8). We then introduced the CRISPRi system targeting *ftsZ* into wild-type ADP1 and a *pbpA* deletion mutant. The strains carrying CRISPRi targeting *gfp* and the strains without the CRISPRi system served as

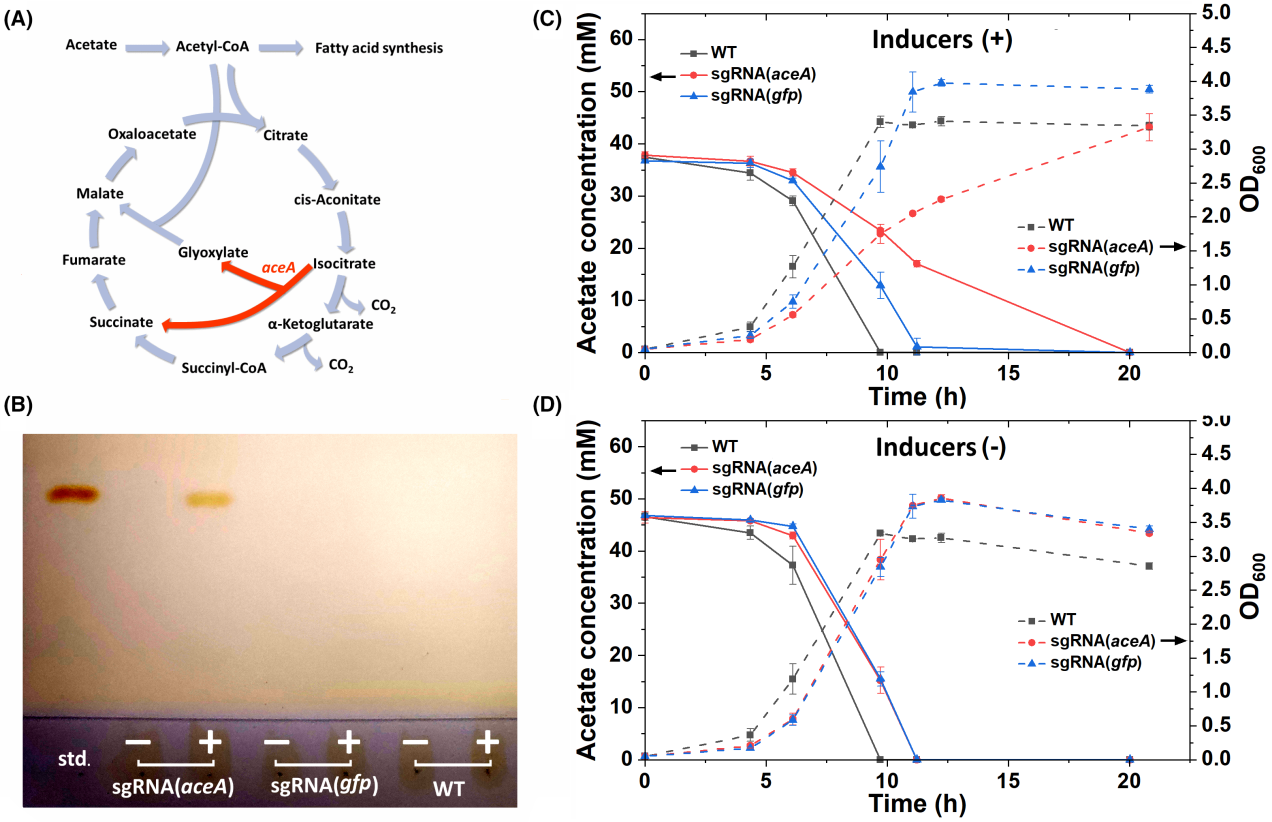

FIGURE 3 Repression of *aceA* by CRISPRi. (A) Schematic of the tricarboxylic acid (TCA) cycle and glyoxylate shunt. The glyoxylate shunt replenishes the TCA cycle intermediates using two molecules of acetate as substrates and is thus essential for cells grown on acetate. The enzyme AceA catalyses the first reaction of the glyoxylate shunt (red). (B) TLC was used to analyse WEs from the biomass at the endpoint (20 h) for each strain with (+) and without (–) inducers. Jojoba oil was used as the standard (std.). Acetate consumption and growth (OD_{600}) of the strain carrying the *aceA*-targeting sgRNA in the presence (C) and absence (D) of inducers are shown. Wild-type (WT) ADP1 and the strain carrying the *gfp*-targeting sgRNA were used as the controls. All the strains were cultivated in MA/9 media supplemented with 40 mM acetate and 0.2% (w/v) casamino acids at 30°C. Data represent average values ± standard deviations of two independent biological experiments.

control strains. We grew cells in LB media and cultivated them at 30°C. Inducers (1% (w/v) arabinose and 5 μM cyclohexanone) were added when cells were in the early exponential phase. Eighteen hours after induction, the cells were investigated through the microscope. The induction led to a significant increase in cell size (determined through the cross-section of single cells on the image) for both, the rod-shaped and spherical strains targeting *ftsZ* (permutation test for both mean and median; *p*-value = 0). For both strains, the median of cell cross-section for randomly selected cell populations under the microscope increased by more than four-fold (Figure 4B,C). Noteworthy, a larger variance in cell size was observed for the population of the rod-shaped strain. Interestingly, in the presence of inducers, the rod-shaped strain continued to elongate as long as nutrients were not limited, while the spherical strain stopped growth at a certain size even with an excess of nutrients. Thus, larger cell size can be obtained in rod-shaped cells than in spherical cells by *ftsZ* repression, and the increment of cell size can be controlled through the induction at different growth stages.

Sedimentation is a cost-efficient method for cell harvesting but usually requires a long sedimentation time (Wang et al., 2019). A larger cell settles faster, given that the density of the single cell is not reduced and is higher than the surrounding fluid. Considering this, we compared the sedimentation of the cells with and without manipulation of cell enlargement. Both, in the rod-shaped and the spherical strains, cell enlargement led to faster sedimentation (Figure 5A,B). Thus, the efficiency of sedimentation can be improved with both elongated rod-shaped and enlarged spherical cells.

Cell enlargement in different cultivation conditions for WE production

Cultivation by co-feeding of glucose and acetate or using only glucose

We next aimed to study the production of WEs in enlarged cells. Although wild-type ADP1 naturally produces wax esters as storage compounds, the

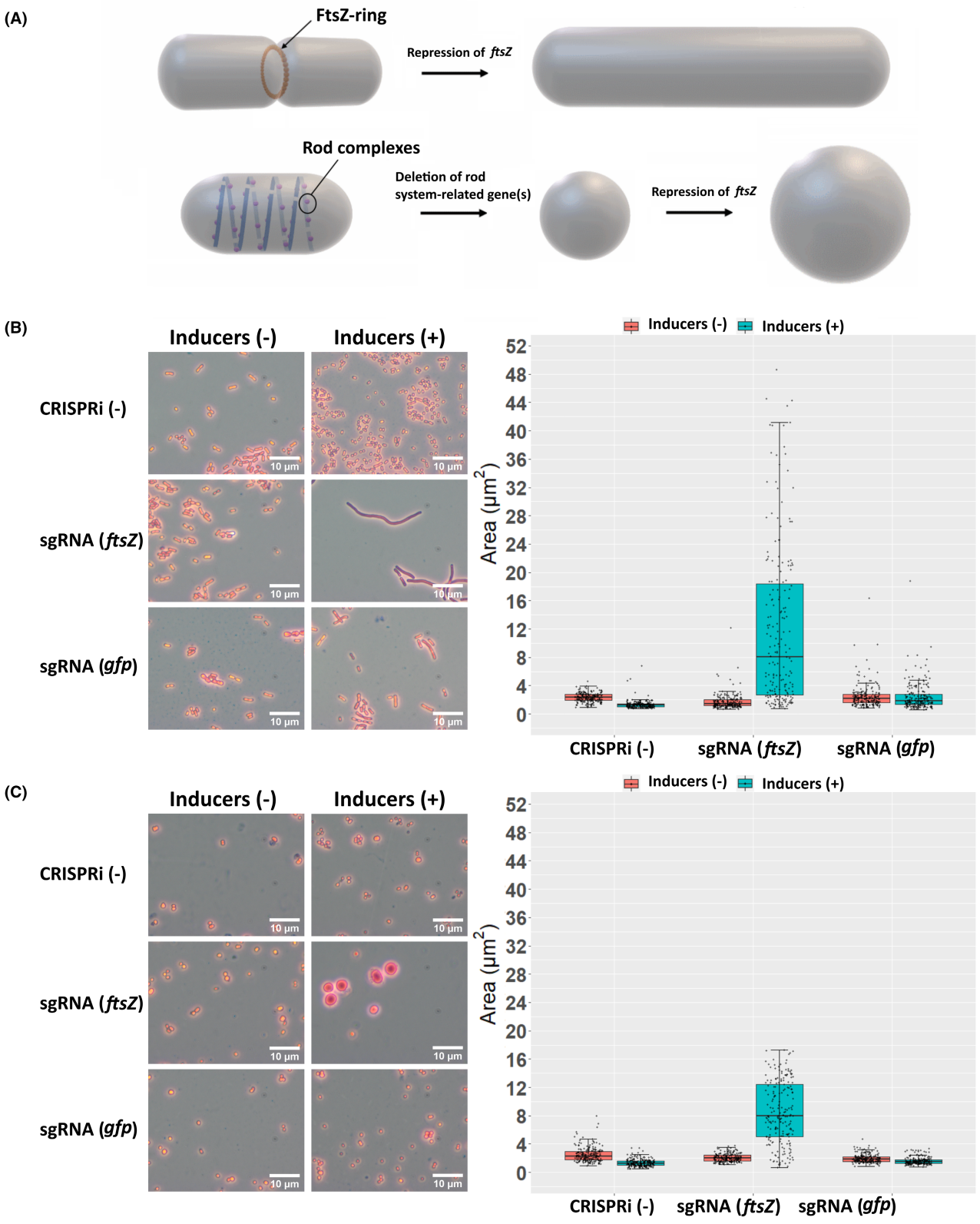

production metrics are low. Previously, co-feeding of a glycolytic carbon source, gluconate, and acetate was performed with ADP1 Δ*aceA* overexpressing *acr1* (Figure 6); the strategy enabled partition of carbon source metabolism such that the glycolytic substrate was used for cell growth while acetate could be directed for WE synthesis, allowing enhanced WE accumulation (Santala et al., 2021). It has also been shown that *aceA* deletion and *acr1* overexpression could lead to improved WE production with high glucose supplementation in the media (Luo et al., 2020). We applied the same engineering strategy in both the

FIGURE 4 Morphological changes and increase of cell size by *ftsZ* repression. (A) Strategies for engineering cell size and shape. The FtsZ-ring is essential for cell division. It acts as the scaffold for recruiting other division proteins and provides contractile force to divide the daughter cells. One model indicates that the MreB polymerizes into long filaments and binds to other peptidoglycan synthesis proteins, such as PBP2 (PbpA) and RodA, to form 'rod complexes'. Deletion of the rod-system-related gene(s) leads to spherical cells. Repression of *ftsZ* in the normal rod-shaped strain led to cell filamentation (B), while *ftsZ* repression in the *pbpA* mutant led to enlarged spherical cells (C). Cells were cultivated in LB media at 30°C. The strains without the CRISPRi machinery and the strains carrying the *gfp*-targeting sgRNA served as controls. Cells were stained with crystal violet before being viewed under the microscope. Two independent biological experiments were performed, from which similar cell morphology changes were observed under the microscope. Photos were shown, and cell size quantification was done for one of the experiments. For each sample, 200 or 300 cells were picked randomly for size analysis, which is shown as the cross-section areas of cells on the images. The data is presented in the boxplot, representing the first quartile (Q1, lower line of the box), the median (Q2, internal line in the box), and the third quartile (Q3, upper line of the box). The lower and upper caps of the vertical lines represent the minimum and maximum respectively. The data point for each cell is overlaid on the boxplot. All the data points outside the vertical lines are outliers, which are data points beyond the 1.5 times interquartile range from either end of the box.

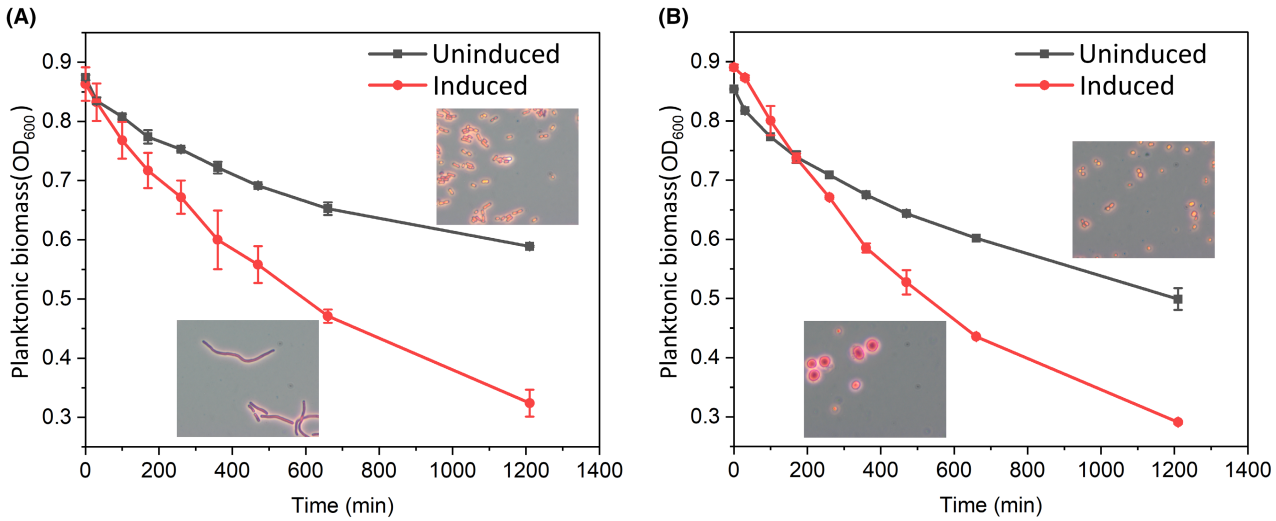

FIGURE 5 Sedimentation of enlarged cells. Sedimentation in both strains, the rod-shaped strain (A) and the *pbpA* mutant (B), was analysed with and without induction of CRISPRi for repression of *ftsZ*. After cultivation in LB media, cells were washed and resuspended in PBS in test tubes. The cells were left undisturbed, and the change of the planktonic biomass (OD_{600}) over time was monitored. Microscope pictures are taken from Figure 4. Two independent sedimentation experiments were performed with the cells from the same culture. Data represent average values ± standard deviations of the two independent sedimentation experiments.

rod-shaped strain and the spherical *pbpA* mutant. The CRISPRi system targeting *ftsZ* was further introduced into the modified strains. The two resulting strains were designated as ASA531 (Δ*aceA* + *acr1* overexpression + CRISPRi targeting *ftsZ*) and ASA532 (Δ*pbpA* + Δ*aceA* + *acr1* overexpression + CRISPRi targeting *ftsZ*). However, it was found that ASA532 had an inconsistent and slower growth than ASA531 when glucose or acetate were supplied in high concentrations (data not shown), thus we focused on ASA531 in the succeeding experiments. Mineral salts media (MSM) was used in all the experiments for WE production.

We first cultivated ASA531 using glucose and acetate as carbon sources; it is expected that cell growth is fuelled by glucose, while WE synthesis is fed by acetate. To ensure a high WE content, we kept a high acetate to glucose ratio; acetate and glucose were added in the beginning with a concentration of 60 and 5 mM, respectively, and were supplied in the same concentrations at 10 and 21 h to avoid depletion of carbon and other components necessary for cellular functions. Three cultures were grown in parallel, in two of which 1% (w/v) arabinose and 50 μM cyclohexanone were added when the OD_{600} of the cells reached ~0.5 (early induction) or ~1.5 (late induction). 50 μM cyclohexanone instead of 5 μM was used to avoid the reduction of induction effect due to potential cyclohexanone evaporation. After 34 h of cultivation, both cultures with induction contained cells with increased size; and cells with early induction were the most elongated (Figure 7A), suggesting that the increase in size can be controlled by the time point of induction. The cellular WE content and titre were found to be approximately 60% higher in the cells with early induction compared to the cells without induction, but the overall WE content for all the cultures was low, less than 6% of the cell dry weight (CDW) (Figure 7B). Looking at the fermentation profiles, the biomass already started to decline for all the cultures after the second carbon source supplementation (~21 h) (Figure S9); meanwhile,

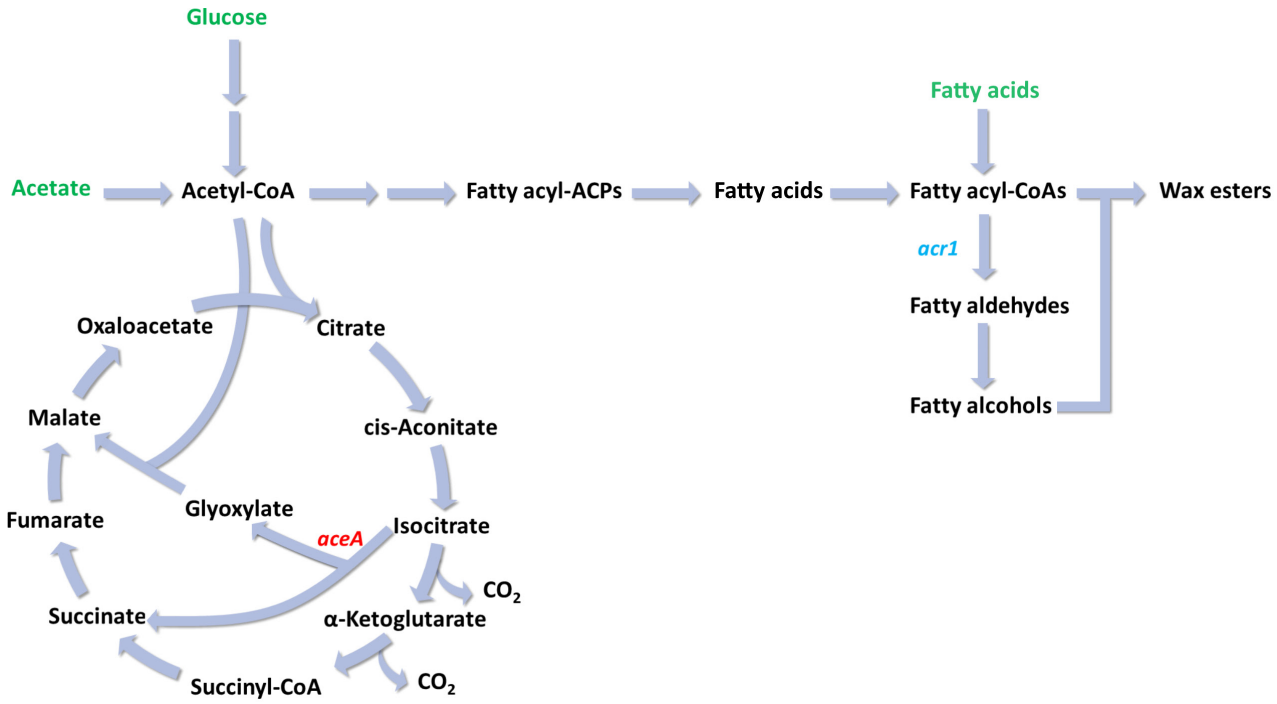

FIGURE 6 Schematic of wax ester (WE) synthesis pathway in ADP1. The substrates used for WE production are highlighted in green. In all the WE production strains used in this study, *aceA*, which encodes isocitrate lyase, was deleted, and *acr1*, which encodes fatty acyl-CoA reductase, was overexpressed. Double arrows indicate that the pathway involves multiple reactions.

glucose consumption almost stopped, and acetate consumption was reduced after 21 h (Figure S9). At the end of the cultivation, all cells consumed 9 mM glucose in total. For the cells without induction, with early induction, and with late induction, the total acetate consumption was 115, 139 and 133 mM respectively (Figure S9).

Therefore, we next cultivated cells in high glucose concentration (200 mM) as this enables cultures to reach higher final biomass concentrations. Induction was performed at higher ODs (OD of ~1.5 for early induction and ~4 for late induction). After 48 h of cultivation, the cells without induction, with early induction and with late induction consumed 124, 118 and 123 mM glucose and reached final ODs of 13.52, 11.6 and 13.1 respectively. In these conditions, the overall WE production was improved for both cultures with and without induction, though the cells with induction produced less WEs (~10% of CDW) compared to the cells without induction (18.5% of CDW) (Figure 7D). However, microscopic analyses (Figure 7C) revealed successful increase of cell size for the cells with induction, thus indicating a higher storage capacity and a potential to further enhance WE accumulation in the enlarged cells.

Cultivation by co-feeding glucose and fatty acids

De novo synthesis of WEs from glucose or acetate involves multiple steps, posing a hindrance to efficient WE accumulation. In addition, the fatty acid synthesis pathway is under tight regulation (Janßen & Steinbüchel, 2014). We hypothesized that by using fatty acids (FAs) as the substrate for WE synthesis (Figure 6), it would be possible to bypass the long synthesis pathway and regulation, and by that circumventing potential inherent limitations for WE synthesis. To this end, we used FAs as the substrate to investigate whether the enlarged cells were capable of storing larger amounts of WEs. In addition, FAs are attractive substrates for WE synthesis as they can be obtained from the hydrolysis of waste cooking oils. Both, ASA531 (Δ*aceA* + *acr1* overexpression + CRISPRi targeting *ftsZ*) and ASA532 (Δ*pbpA* + Δ*aceA* + *acr1* overexpression + CRISPRi targeting *ftsZ*), were cultivated in media containing 10 mM glucose and ~14 g/L FAs (mainly oleic acid: 65%–88%). At 12 h, 10 mM glucose was supplemented, and inducers were added for cell enlargement. After 36 h of cultivation, the enlarged cells were found to accumulate a large amount of lipid droplet, observed by microscopic analysis (Figure 7E). The identity of the lipid droplets was validated by Nile red staining (Figure 7E). Interestingly, for both cultures with and without induction, a part of the cells could not be sedimented by centrifugation and was suspended in or floating on top of the media (Figure S10). This could result from the use of fatty acids as the substrate, which may reduce the density of single cells (or cell-matrix). The density can also be reduced due to increased WE accumulation, as the cells (with *ftsZ* repression) in

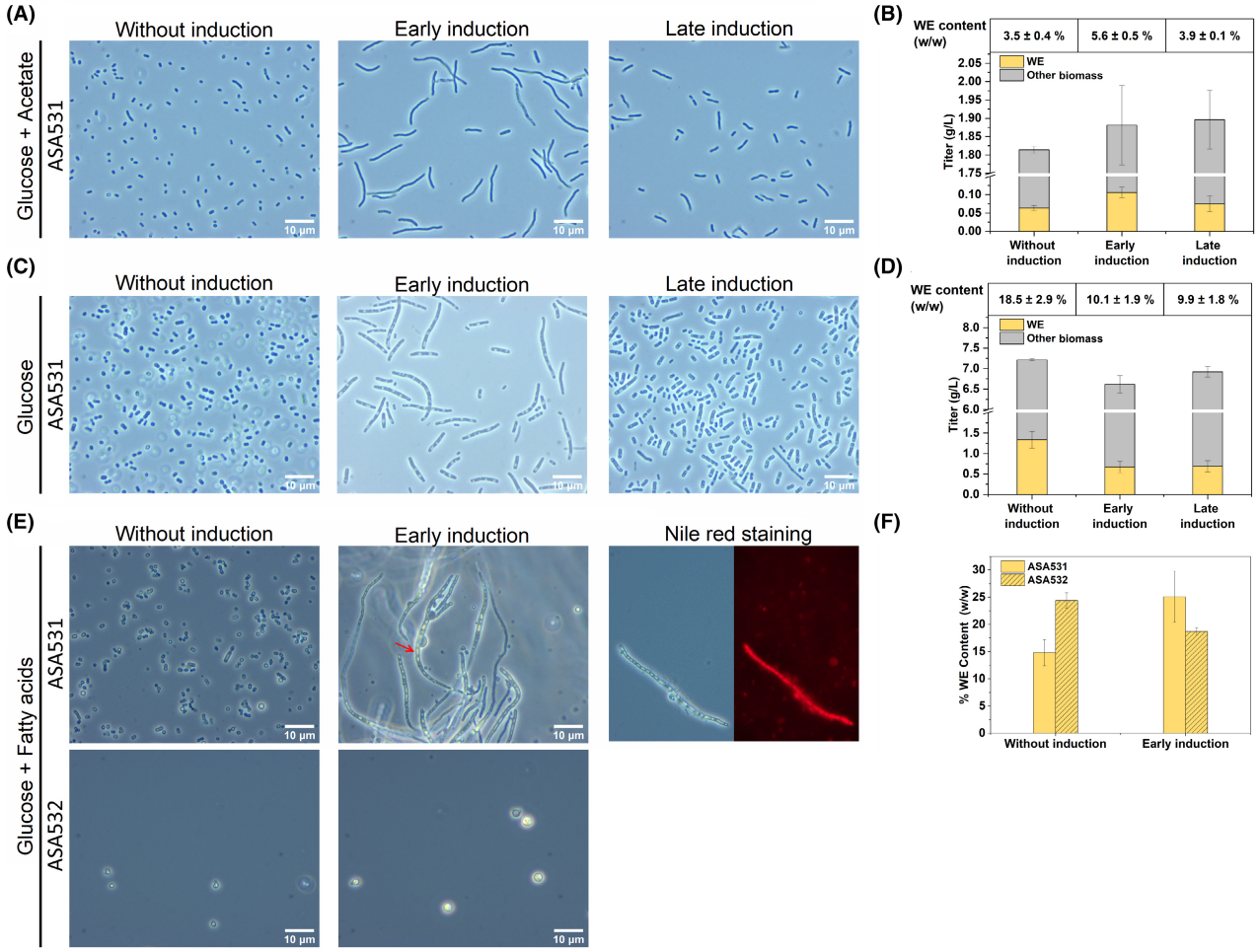

FIGURE 7 Wax ester (WE) production by enlarged cells in different conditions. (A) Morphology change of the strain ASA531 after *ftsZ* repression when cultivated by co-feeding of glucose and acetate; the corresponding production metrics are shown in (B). (C) Morphology change of the strain ASA531 after *ftsZ* repression when cultivated with glucose; the corresponding production metrics are shown in (D). (E) Morphology change of the strains ASA531 and ASA532 after *ftsZ* repression when cultivated by co-feeding of glucose and fatty acids; under this condition, a part of cells was floating on the media after centrifugation, and only the cell pellets were collected for WE quantification and the corresponding contents were shown in (F). Lipid droplets (red arrow) were visible in the enlarged cells cultivated with fatty acids under the microscope. Nile red was used to stain the lipid body. Data represent average values ± standard deviations of two independent biological experiments. An average WE molecular weight of 506 g/mol (corresponding to 34 carbons and one double bond) was used for WE quantification.

the low-density fraction seemed to accumulate more lipid based on microscopic observation (Figure S11). Eventually, only the part of the cells that were collected by centrifugation was subjected to WE quantification. According to WE quantification, the enlarged cells of ASA531 accumulated WEs up to 25.1% of CDW, which was higher than the content of the cells without induction (14.8% of CDW; Figure 7F). However, the enlarged ASA532 had lower WE content (18.7% of CDW) than the ASA532 cells without induction (24.4% of CDW; Figure 7F). The WE content might be slightly underestimated as we used the previously determined the average molecular weight of WEs of 506 g/mol, corresponding to 34 carbons (Lehtinen et al., 2018). Here, the supplementation of the fatty acid substrate, mostly consisting of oleic acid (18 carbons), may increase the average WE molecular weight.

The WE quantification is conventionally done by cell collection, cell dry weight determination and lipid extraction followed by NMR analysis (Santala, Efimova, Karp, et al., 2011). However, in this specific case, the low-density cell fraction was loosely packed on top of the media, and consequently it was difficult to collect the low-density cells and wash them to remove impurities such as fatty acid and other medium residues. Nevertheless, we carried out a similar cultivation by co-feeding of glucose and fatty acids (with a longer cultivation time of 48 h) and determined the WE titres by directly freeze-drying the whole cultures. Considering that early induction may lead to a low biomass formation, induction was performed at different time points (14, 22 and 28 h). After the cultivation, the cultures were freeze-dried for 48 h. The dry matters contained both cells and other medium residues. The total dry matters

were subjected to lipid extraction. The amounts of dry matter from the cultures with induction was higher than that from the culture without induction (Figure 8). The difference in the amount of dry matter can be explained by the presence of arabinose in the cultures with induction and the difference in carbon utilization between different cultures, which could lead to the release of different amount of carbon dioxide. NMR analysis for the lipid extracts showed that a WE titre of 1.24 g/L was produced from the culture without induction (Figure 8). The culture with induction at 14 h produced the lowest WE titre of 0.51 g/L (Figure 8), which can be partially explained by the low amount of biomass. The WE titre was increased to 0.72 and 1.39 g/L for the cultures induced at 22 and 28 h (Figure 8).

DISCUSSION

The development of cell factories that meet economic requirements for industrial production needs significant research efforts. For intracellular products, it can be even more challenging due to the high cost of product recovery. The cost of the downstream processes, which can contribute to more than 70% of the total production cost, can be significantly reduced if high biomass titre and product content are achieved, and thus less effort is needed for the biomass and product collection (Yenkie et al., 2017). However, the accumulation of intracellular products can be limited due to the small size of bacterial cells. Larger cells provide more space for product accumulation and can thus be more efficient for production (Jiang & Chen, 2016; Wang et al., 2019).

In addition, cell size can have a great influence on cell harvesting. For example, large-sized cells may be more effectively separated by filtration or enable a faster sedimentation rate (Wang et al., 2019; Yenkie et al., 2017). Elongated *E. coli* cells, engineered to accumulated polyhydroxyalkanoates (PHAs) are able to settle after 20 min (Wang et al., 2014). In the current study, both the elongated rod-shaped cells and the enlarged spherical cells settled faster than the normal-sized cells because the settling velocity is proportional to the square of the particle radius according to Stokes' law. It should be noted, however, that the difference in densities between the microorganisms and the surrounding fluid is also an important factor affecting the settling velocity, and the density of microorganisms can be affected by the accumulated intracellular products. Accumulation of products that are denser than the cells, such as PHB, glycogen and sulphur, will increase the density of microorganisms (Mas et al., 1985), thus increasing the settling velocity. In contrast, the accumulation of low-density products, such as WEs in the current study, can decrease the density of cells, and sedimentation may not benefit from large-sized cells.

Here, inducible CRISPRi offers a convenient way to modulate gene expression for cell size control, as this modulation often reduce the fitness of the cells severely and therefore a permanent change is deleterious. Furthermore, the system is well suited for a broad range of engineering purposes and functional studies for essential genes. Previously, CRISPRi was used in *A. baylyi* ADP1 to repress the activity of IS elements, enabling a reduction of mutation rate (Geng et al., 2019). However, both *dCas9* and the sgRNAs were constitutively expressed, which limits its application to non-essential genes. To suppress cell division, we first established an inducible CRISPRi system. The sgRNA was expressed in a medium-copy pBAV plasmid (Bryksin & Matsumura, 2010), while *dCas9* was integrated into the genome to reduce plasmid size and alleviate its potential toxicity caused by high dosage (Zhang & Voigt, 2018). The spacer sequence in the sgRNA can be easily replaced by PCR-based methods. In the previously described inducible CRISPRi systems,

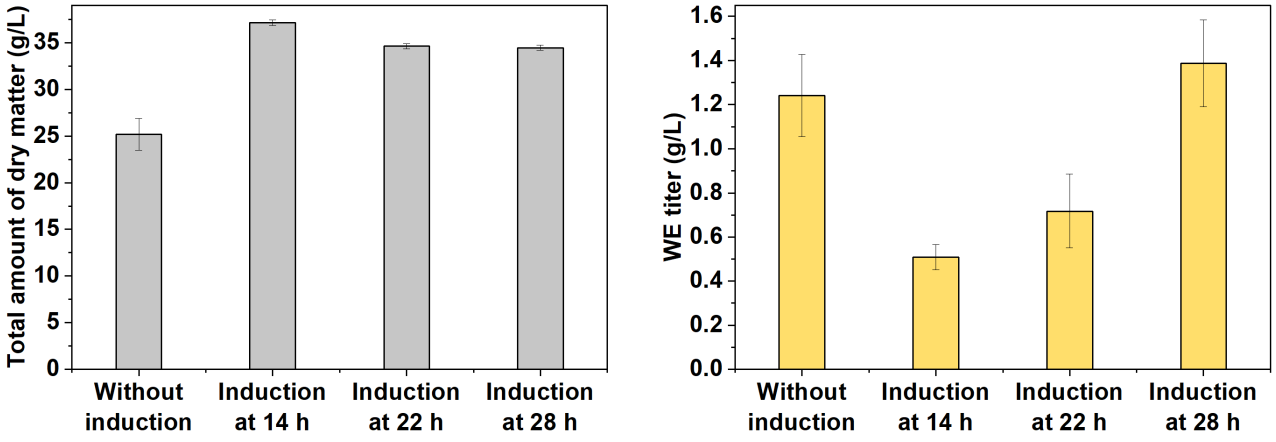

FIGURE 8 WE quantification after freeze-drying the whole cell cultures. The total amounts of dry matter for the cultures without induction and with induction at different time points are presented in the left panel. The corresponding wax ester (WE) titres are shown in the right panel. Data represent average values ± standard deviations of two independent biological experiments. An average WE molecular weight of 506 g/mol (corresponding to 34 carbons and one double bond) was used for WE quantification.

an inducible promoter was usually used to control the expression of dCas9 while sgRNA was expressed constitutively (Guzzo et al., 2020; Li et al., 2016; Peters et al., 2016; Qi et al., 2013; Woolston et al., 2018). However, such systems can lead to leaky repression (Li et al., 2016; Peters et al., 2016). Here, to minimize the leakage, we used two inducible promoters, namely the arabinose-inducible promoter P_{araBAD} and the cyclohexanone-inducible promoter P_{chnB}, to control the expression of the sgRNA and *dCas9* separately. The arabinose-inducible promoter is widely used for the expression of heterologous genes. In ADP1, arabinose can be unselectively oxidized by glucose dehydrogenase in the absence of glucose (Kannisto et al., 2015; Santala et al., 2018), which may reduce the effect of induction. This feature has been exploited to create an autonomously regulated switch for gene expression regulation (Santala et al., 2018) and could also be coupled with CRISPRi to make it even more dynamic. On the other hand, the oxidation of arabinose can be readily relieved by supplementing cells with glucose. The cyclohexanone-inducible promoter is originated from a cluster of genes responsible for cyclohexanol degradation in *A. johnsonii*, regulated by its cognate activator ChnR (Steigedal & Valla, 2008).

Studying essential genes by CRISPRi is highly sensitive to perturbations; leakage of the repression system, for example, can severely impair cell growth. We showed that the employment of the two induction systems enables a tightly controlled CRISPRi system. Due to the leakiness of both inducible promoters, expression of either the sgRNA or the dCas9 can lead to a moderate repression level. In the absence of both inducers, the established CRISPRi exhibits minimal leaky repression, as indicated by the unchanged phenotypes. In addition, the burden of CRISPRi was significantly reduced by optimizing the dCas9 dosage. The minimized burden is important for gene repression study, especially when exploring how the repression of a specific gene affects cell morphology, which can be easily influenced by cell physiological conditions (Si et al., 2017).

It is also worth mentioning that recently the native CRISPR system of ADP1 was also shown to be functional (Suárez et al., 2020). However, it is unlikely that the native ADP1 Cas protein binds to the sgRNAs used here. For example, the native Cas system in ADP1 is Type I-Fa and should recognize a different PAM site.

The ability to simultaneously target multiple loci will expand the application of CRISPRi. Multiplex CRISPRi enables systematic genetic interaction studies (Guzzo et al., 2020). To enhance metabolic flux towards desired products by metabolic engineering, modulation of the expression of multiple genes is often required. For example, simultaneous repression of four competing pathway genes increased the yield and productivity of n-butanol in *E. coli* (Kim et al., 2017). In addition, the expression of multiple sgRNAs targeting the same gene can improve the repression efficiency for this gene (McCarty et al., 2019). Thus, we were keen to explore multiplex CRISPRi in ADP1. Targeting multiple loci requires the expression of multiple sgRNAs. This can be accomplished by the expression of each sgRNA using an individual promoter. Alternatively, the expression platform can be composed of a single promoter and a guide RNA array, which is processed into multiple functional sgRNAs. The former strategy is straightforward and has been used in many studies (Geng et al., 2019; Guzzo et al., 2020; Kim et al., 2016). However, repeated use of the same promoter may trigger genetic instability due to homologous recombination. Thus, we chose to use one promoter to express a sgRNA array encoding multiple sgRNAs. Processing of the single transcript into functional sgRNAs was achieved by co-expression of the ribonuclease Cas6 (Haurwitz et al., 2010), which cleaves RNA on specific sites inserted between sgRNA sequences. Cas6 is part of the native CRISPR system in *P. aeruginosa*, responsible for processing CRISPR transcripts. Besides, Cas6 functions in various other organisms, including *E. coli*, *Bacillus subtilis* and *Saccharomyces cerevisiae* (Qi et al., 2012). Other strategies for processing guide RNA arrays have been summarized in McCarty et al. (2020), such as the employment of a CRISPR effector possessing RNase activity, for example, Cas12a. Here, we established a multiplex CRISPRi system in ADP1 for the first time. The system was successfully used to simultaneously repress *gfp* and *mScarlet*. Besides, it was found that the unprocessed guide RNA array was still effective in guiding the repression of *gfp* even in the absence of Cas6. The observation indicated that the function of the *gfp*-targeting sgRNA (the first sgRNA in the array) in the unprocessed transcript was not affected by the 32 mismatched nucleotides upstream of the base-pairing region and the succeeding sequence of the *mScarlet*-targeting sgRNA (the second sgRNA in the array). A study in HEK293FT cells showed that extension of sgRNA guiding sequences beyond the 20 bp did not influence targeting specificity, which was due to the sgRNA being processed to contain the 20 bp guiding sequence (Ran et al., 2013). It was also shown in *E. coli* that extensions to the base-pairing region with mismatched nucleotides do not completely abort the sgRNA function, though the repression efficiency can be significantly reduced (Larson et al., 2013). However, it remains unclear how the succeeding sequence of the second sgRNA does not affect the function of the first sgRNA in the unprocessed transcript. One possibility is that the *gfp*-targeting sgRNA was transcribed separately without the succeeding sequence because of the presence of the transcription terminator from *Streptococcus pyogenes* in the sgRNA scaffold (Larson et al., 2013), though the seven consecutive Us originally succeeding the terminator are not present in the construct of the current study.

The utility of the CRISPRi to modulate cell metabolism in ADP1 was first evaluated by repressing the expression of *aceA*, an isocitrate lyase catalysing the first reaction of the glyoxylate shunt. The significance of the glyoxylate shunt downregulation in metabolic engineering has been shown in our previous study, where the carbon flux could be redirected from biomass formation to wax ester synthesis when acetate was used as the substrate (Santala et al., 2018). We observed that *aceA* repression specifically decreased acetate consumption and cell growth rates when cells were grown in the media containing casamino acids and acetate, indicating a lowered carbon flux from acetate to biomass and direction of carbon to WEs. The results suggest that the CRISPRi system could be used as an efficient tool for pathway optimization and conditional regulation of gene expression in metabolic engineering.

For increasing the cell size, we conditionally suppressed cell division by repressing *ftsZ* expression using the inducible CRISPRi. FtsZ is critical for cell division and has been used as an effective target for cell size engineering in *E. coli* (Ding et al., 2020; Elhadi et al., 2016; Jiang & Chen, 2016). Suppression of cell division can also be achieved by overexpression of the genes coding negative regulatory proteins such as SulA and MinC (Ding et al., 2020; Wang et al., 2014), both inhibiting FtsZ assembly. Here, *ftsZ* repression resulted in cell elongation for the rod-shaped strain and enlarged spherical cells for the spherical strain (with *pbpA* deletion). Notably, the induction was effective throughout the whole population, leading to an increase in cell size for the majority of the cell population. With the repression of *ftsZ*, the rod-shaped strain can continue elongating to form a very long filament. The elongation can lead to a decreased SA/V even when the cell width is not changed. In contrast, the spherical strain will stop growing after the cell reach a certain size, leading to a narrower range of cell size compared to the rod-shaped strain. Compared to cell filamentation, enlargement of a spherical cell with the same volume decreases the SA/V to a larger degree. However, a too low SA/V may result in reduced cell fitness, given that the diffusion of nutrients from external environment can be constrained by small surface area (Young, 2006).

WEs are high-value lipids which can be used in a broad range of applications, such as cosmetics, pharmaceuticals and lubricants (Bart et al., 2013; Fiume et al., 2015; Gad et al., 2021). ADP1 naturally accumulates WEs as storage compounds. Their synthesis is initiated at the cytoplasm membrane, followed by the formation of matured lipid bodies. WE or other neutral lipid synthesis has not been previously investigated in cells with altered morphology. In previous studies, WEs have been proposed to be even toxic in some hosts (Kaiser et al., 2013), potentially due to the lack of proper organization of the lipid bodies in the cells. Therefore, it was unclear whether the cells with altered morphology could sustain WE production. Interestingly, the engineered cells could produce WEs intracellularly, including strains with the upregulated WE synthesis pathway. In the cultivation with co-fed glucose and acetate, the elongated cells showed slightly higher WE content, though both the normal-sized cells and the elongated cells had low WE contents. This might have to do with cell lysis, as it was observed that the OD of the cultures had already declined to a fair extent when cells were harvested for WE quantification. While acetate was present in excess throughout the cultivation, glucose was almost depleted at 21 h. Rather than the morphology changes, the depletion of glucose might be the reason for cell lysis because the cellular metabolism was not sustained, and acetate alone did not support cell growth due to *aceA* deletion. Although glucose was supplemented again at 21 h, it was not consumed by the cells. It is thus important to employ a constant feeding strategy to avoid nutrient depletion, as has been done previously (Santala et al., 2021). We then cultivated the cells with high glucose concentration; the WE content of the elongated cells was increased but was lower than that of the normal-sized cells. De novo WE synthesis could be largely affected by the cell fitness, due to the long and tightly regulated pathway; compared to the normal-sized cells, the elongated cells may be of decreased fitness due to the potential burden by the expression of the CRISPRi machinery and less efficient nutrient intake. Another potential factor could be the reduced formation of cell surface, since WE synthesis was reported to be membrane-associated (Stöveken et al., 2005; Wältermann et al., 2005).

To further investigate the capacity of the enlarged cells to accumulate larger amounts of WEs, we used a shortcut synthesis pathway to WEs by directly providing cells with FAs. The strategy bypasses the energetically uphill and regulated fatty acid synthesis pathway. In addition, FAs can be easily obtained by hydrolysis of waste cooking oils, which could offer a feasible feedstock for the biological production of high-value chemicals. The use of FAs enhanced WE accumulation in the elongated cells, as indicated by the formation of a large amount of lipid body that was visible under the microscope and confirmed by Nile red staining. Furthermore, WE accumulation displayed heterogeneity between elongated cells; while some cells bulged due to lipid accumulation, others still held potential storage capacity. Despite the drastic phenotypic change, the elongated cells sustained efficient WE synthesis, highlighting the advantage of large cells for accumulating intracellular products; the elongated cells (ASA531 with induction) were found to accumulate ~70% more WEs than the normal-sized cells, despite the fact that only part of the cells could be centrifuged and analysed. It should be noted that, for both elongated and normal-sized cells, the low-density cell fraction that was floating on the media can have a higher WE content. In addition, it

was concluded that elongated cells work better than enlarged spherical cells with respect to WE production, though enlarged spherical cells might also be advantageous in other applications. In the attempt to demonstrate the WE storage capacity of elongated cells, induction for *ftsZ* repression was performed at an early stage; while the growth would be stalled to some degree due to *ftsZ* repression, the shortcut WE synthesis could be less affected, consequently resulting in higher content. However, the strategy led to a lower titre as a trade-off. Thus, proper timing of induction is important to reach a balance between titre and content, as demonstrated by the experiment in which a higher titre was obtained with later induction. Although fatty acids were shown to provide a shortcut for WE synthesis, the current production strain has not been optimized for fatty acid utilization and there is still potential to further improve the efficiency of WE synthesis. Therefore, further metabolic engineering efforts are required to harness the benefits of the increased storage capacity of large-sized cells. Overall, the current study demonstrated cell morphology engineering as a potential strategy for improving WE production.

CONCLUSION

In this study, an inducible and tightly controlled CRISPRi system was established in *A. baylyi* ADP1, allowing the investigation and repression of growth-essential genes for desired phenotype changes. To expand the application of the CRISPRi system, multiplex gene repression was explored by using a multiple sgRNA expression strategy based on the ribonuclease Cas6. The established CRISPRi system was further used for pathway modulation and cell morphology engineering. The cell size of *A. baylyi* ADP1 was increased by repressing *ftsZ*, an essential gene for cell division. Despite the cell division being severely perturbed by CRISPRi, the engineered cells were able to sustain high WE production and accumulated up to 25% WEs of cell dry weight. Furthermore, the microscopic analyses indicated that even higher storage capacity could be harnessed for WE accumulation. Our results demonstrate the benefit of the inducible CRISPRi system for a variety of applications, including genome-scale gene functional study and metabolic engineering in ADP1, and warrant further studies on large-sized cells for the production of the high-value intracellular product, wax esters.

AUTHOR CONTRIBUTIONS

JL, SS, and VS designed the study. JL, SS, EE, and DCV carried out the research work. JL, SS, VS, and DCV analysed the data. SS and VS supervised the study. All authors participated in writing the manuscript. All authors read and approved the final manuscript.

AUTHOR CONTRIBUTIONS ACKNOWLEDGEMENTS

The financial support from The Novo Nordisk Foundation through grants NNF20CC0035580 and TARGET (NNF21OC0067996), and the European Union's Horizon 2020 Research and Innovation Programme under grant agreement No. 814418 (SinFonia) to the Systems Environmental Microbiology laboratory is gratefully acknowledged. Part of this work was carried out by S. Santala in the Systems Environmental Microbiology laboratory at The Novo Nordisk Foundation for Biosustainability in the context of a research stay supported by Academy of Finland (grant no. 310135).

FUNDING INFORMATION

The work presented in this article is supported by Academy of Finland (grants no. 334822, 310188) and The Novo Nordisk Foundation grant NNF21OC0067758.

CONFLICT OF INTEREST

The authors declare no conflict of interest.

DATA AVAILABILITY STATEMENT

The datasets used and analyzed during the current study are available from the corresponding author on reasonable request.

ORCID

Jin Luo https://orcid.org/0000-0001-6126-9394
Daniel Christoph Volke https://orcid.org/0000-0003-0244-2534
Ville Santala https://orcid.org/0000-0002-9084-931X
Suvi Santala https://orcid.org/0000-0002-0047-5319

REFERENCES

Bae, S., Park, J. & Kim, J.-S. (2014) Cas-OFFinder: a fast and versatile algorithm that searches for potential off-target sites of Cas9 RNA-guided endonucleases. *Bioinformatics*, 30, 1473–1475.

Bart, J.C.J., Gucciardi, E. & Cavallaro, S. (2013) Renewable feedstocks for lubricant production. In: *Biolubricants*. Bart, J.C.J., Gucciardi, E. & Cavallaro, S. (eds). Sawston, United Kingdom: Woodhead Publishing, pp. 121–248.

Biggs, B.W., Bedore, S.R., Arvay, E., Huang, S., Subramanian, H., McIntyre, E.A. et al. (2020) Development of a genetic toolset for the highly engineerable and metabolically versatile Acinetobacter baylyi ADP1. *Nucleic Acids Research*, 48, 5169–5182.

Brockman, I.M. & Prather, K.L.J. (2015a) Dynamic knockdown of *E. coli* central metabolism for redirecting fluxes of primary metabolites. *Metabolic Engineering*, 28, 104–113.

Brockman, I.M. & Prather, K.L.J. (2015b) Dynamic metabolic engineering: new strategies for developing responsive cell factories. *Biotechnology Journal*, 10, 1360–1369.

Bryksin, A.V. & Matsumura, I. (2010) Rational design of a plasmid origin that replicates efficiently in both gram-positive and gram-negative bacteria. *PLoS One*, 5, e13244.

Carballido-López, R. (2019) Rod width under control. *Nature Microbiology*, 4, 1246–1248.

Cho, H., Wivagg, C.N., Kapoor, M., Barry, Z., Rohs, P.D.A., Suh, H. et al. (2016) Bacterial cell wall biogenesis is mediated by SEDS and PBP polymerase families functioning semi-autonomously. *Nature Microbiology*, 1, 16172.

Cuff, L.E., Elliott, K.T., Seaton, S.C., Ishaq, M.K., Laniohan, N.S., Karls, A.C. et al. (2012) Analysis of IS1236-mediated gene amplification events in *Acinetobacter baylyi* ADP1. *Journal of Bacteriology*, 194, 4395–4405.

Ding, Q., Ma, D., Liu, G.-Q., Li, Y., Guo, L., Gao, C. et al. (2020) Light-powered *Escherichia coli* cell division for chemical production. *Nature Communications*, 11, 2262.

Elhadi, D., Lv, L., Jiang, X.-R., Wu, H. & Chen, G.-Q. (2016) CRISPRi engineering *E. coli* for morphology diversification. *Metabolic Engineering*, 38, 358–369.

Fiume, M.M., Heldreth, B.A., Bergfeld, W.F., Belsito, D.V., Hill, R.A., Klaassen, C.D. et al. (2015) Safety assessment of alkyl esters as used in cosmetics. *International Journal of Toxicology*, 34, 5S–69S.

Gad, H.A., Roberts, A., Hamzi, S.H., Gad, H.A., Touiss, I., Altyar, A.E. et al. (2021) Jojoba oil: an updated comprehensive review on chemistry, pharmaceutical uses, and toxicity. *Polymers*, 13, 1711.

Geng, P., Leonard, S.P., Mishler, D.M. & Barrick, J.E. (2019) Synthetic genome defenses against selfish DNA elements stabilize engineered bacteria against evolutionary failure. *ACS Synthetic Biology*, 8, 521–531.

Guzzo, M., Castro, L.K., Reisch, C.R., Guo, M.S. & Laub, M.T. (2020) A CRISPR interference system for efficient and rapid gene knockdown in *Caulobacter crescentus*. *mBio*, 11, 1–16.

Haurwitz, R.E., Jinek, M., Wiedenheft, B., Zhou, K. & Doudna, J.A. (2010) Sequence- and structure-specific RNA processing by a CRISPR endonuclease. *Science*, 329, 1355–1358.

Hou, J., Gao, C., Guo, L., Nielsen, J., Ding, Q., Tang, W. et al. (2020) Rewiring carbon flux in *Escherichia coli* using a bifunctional molecular switch. *Metabolic Engineering*, 61, 47–57.

Janßen, H.J. & Steinbüchel, A. (2014) Fatty acid synthesis in *Escherichia coli* and its applications towards the production of fatty acid based biofuels. *Biotechnology for Biofuels*, 7, 7.

Jiang, X.R. & Chen, G.Q. (2016) Morphology engineering of bacteria for bio-production. *Biotechnology Advances*, 34, 435–440.

Jiang, W., Bikard, D., Cox, D., Zhang, F. & Marraffini, L.A. (2013) RNA-guided editing of bacterial genomes using CRISPR-Cas systems. *Nature Biotechnology*, 31, 233–239.

Kaiser, B.K., Carleton, M., Hickman, J.W., Miller, C., Lawson, D., Budde, M. et al. (2013) Fatty aldehydes in cyanobacteria are a metabolically flexible precursor for a diversity of biofuel products. *PLoS One*, 8, e58307.

Kannisto, M.S., Mangayil, R.K., Shrivastava-Bhattacharya, A., Pletschke, B.I., Karp, M.T. & Santala, V.P. (2015) Metabolic engineering of *Acinetobacter baylyi* ADP1 for removal of Clostridium butyricum growth inhibitors produced from lignocellulosic hydrolysates. *Biotechnology for Biofuels*, 8, 198.

Kim, S.K., Han, G.H., Seong, W., Kim, H., Kim, S.-W., Lee, D.-H. et al. (2016) CRISPR interference-guided balancing of a biosynthetic mevalonate pathway increases terpenoid production. *Metabolic Engineering*, 38, 228–240.

Kim, S.K., Seong, W., Han, G.H., Lee, D.-H. & Lee, S.-G. (2017) CRISPR interference-guided multiplex repression of endogenous competing pathway genes for redirecting metabolic flux in Escherichia coli. *Microbial Cell Factories*, 16, 188.

Kocaoglu, O. & Carlson, E.E. (2015) Profiling of β-lactam selectivity for penicillin-binding proteins in Escherichia coli strain DC2. *Antimicrobial Agents and Chemotherapy*, 59, 2785–2790.

Kozaeva, E., Volkova, S., Matos, M.R.A., Mezzina, M.P., Wulff, T., Volke, D.C. et al. (2021) Model-guided dynamic control of essential metabolic nodes boosts acetyl-coenzyme A–dependent bioproduction in rewired pseudomonas putida. *Metabolic Engineering*, 67, 373–386.

Larson, M.H., Gilbert, L.A., Wang, X., Lim, W.A., Weissman, J.S. & Qi, L.S. (2013) CRISPR interference (CRISPRi) for sequence-specific control of gene expression. *Nature Protocols*, 8, 2180–2196.

Lehtinen, T., Santala, V. & Santala, S. (2017) Twin-layer biosensor for real-time monitoring of alkane metabolism. *FEMS Microbiology Letters*, 364, 1–7.

Lehtinen, T., Efimova, E., Santala, S. & Santala, V. (2018) Improved fatty aldehyde and wax ester production by overexpression of fatty acyl-CoA reductases. *Microbial Cell Factories*, 17, 19.

Li, X.T., Jun, Y., Erickstad, M.J., Brown, S.D., Parks, A., Court, D.L. et al. (2016) TCRISPRi: tunable and reversible, one-step control of gene expression. *Scientific Reports*, 6, 1–12.

Losoi, P.S., Santala, V.P. & Santala, S.M. (2019) Enhanced population control in a synthetic bacterial consortium by interconnected carbon cross-feeding. *ACS Synthetic Biology*, 8, 2642–2650.

Luo, J., Lehtinen, T., Efimova, E., Santala, V. & Santala, S. (2019) Synthetic metabolic pathway for the production of 1-alkenes from lignin-derived molecules. *Microbial Cell Factories*, 18, 48.

Luo, J., Efimova, E., Losoi, P., Santala, V. & Santala, S. (2020) Wax ester production in nitrogen-rich conditions by metabolically engineered *Acinetobacter baylyi* ADP1. *Metabolic Engineering Communications*, 10, e00128.

Makarova, K.S., Haft, D.H., Barrangou, R., Brouns, S.J.J., Charpentier, E., Horvath, P. et al. (2011) Evolution and classification of the CRISPR–Cas systems. *Nature Reviews. Microbiology*, 9, 467–477.

Martin, L.K., Huang, W.E. & Thompson, I.P. (2021) Bacterial wax synthesis. *Biotechnology Advances*, 46, 107680.

Mas, J., Pedrós-Alió, C. & Guerrero, R. (1985) Mathematical model for determining the effects of intracytoplasmic inclusions on volume and density of microorganisms. *Journal of Bacteriology*, 164, 749–756.

McCarty, N.S., Shaw, W.M., Ellis, T. & Ledesma-Amaro, R. (2019) Rapid assembly of gRNA arrays via modular cloning in yeast. *ACS Synthetic Biology*, 8, 906–910.

McCarty, N.S., Graham, A.E., Studená, L. & Ledesma-Amaro, R. (2020) Multiplexed CRISPR technologies for gene editing and transcriptional regulation. *Nature Communications*, 11, 1281.

Metzgar, D. (2004) Acinetobacter sp. ADP1: an ideal model organism for genetic analysis and genome engineering. *Nucleic Acids Research*, 32, 5780–5790.

Murin, C.D., Segal, K., Bryksin, A. & Matsumura, I. (2012) Expression vectors for *Acinetobacter baylyi* ADP1. *Applied and Environmental Microbiology*, 78, 280–283.

Peters, J.M., Colavin, A., Shi, H., Czarny, T.L., Larson, M.H., Wong, S. et al. (2016) A comprehensive, CRISPR-based functional analysis of essential genes in bacteria. *Cell*, 165, 1493–1506.

Qi, L., Haurwitz, R.E., Shao, W., Doudna, J.A. & Arkin, A.P. (2012) RNA processing enables predictable programming of gene expression. *Nature Biotechnology*, 30, 1002–1006.

Qi, L.S., Larson, M.H., Gilbert, L.A., Doudna, J.A., Weissman, J.S., Arkin, A.P. et al. (2013) Repurposing CRISPR as an RNA-guided platform for sequence-specific control of gene expression. *Cell*, 152, 1173–1183.

Ran, F.A., Hsu, P.D., Lin, C.-Y., Gootenberg, J.S., Konermann, S., Trevino, A.E. et al. (2013) Double nicking by RNA-guided CRISPR Cas9 for enhanced genome editing specificity. *Cell*, 154, 1380–1389.

Santala, S. & Santala, V. (2021) Acinetobacter baylyi ADP1—naturally competent for synthetic biology. *Essays in Biochemistry*, 65, 309–318.

Santala, S., Efimova, E., Karp, M. & Santala, V. (2011) Real-time monitoring of intracellular wax ester metabolism. *Microbial Cell Factories*, 10, 75.

Santala, S., Efimova, E., Kivinen, V., Larjo, A., Aho, T., Karp, M. et al. (2011) *Improved triacylglycerol production in Acinetobacter baylyi* ADP1 by metabolic engineering. *Microbial Cell Factories*, 10, 36.

Santala, S., Efimova, E., Koskinen, P., Karp, M.T. & Santala, V. (2014) Rewiring the wax Ester production pathway of *Acinetobacter baylyi* ADP1. *ACS Synthetic Biology*, 3, 145–151.

Santala, S., Karp, M. & Santala, V. (2014) Rationally engineered synthetic coculture for improved biomass and product formation. *PLoS One*, 9, e113786.

Santala, S., Efimova, E. & Santala, V. (2018) Dynamic decoupling of biomass and wax ester biosynthesis in Acinetobacter baylyi by an autonomously regulated switch. *Metabolic Engineering Communications*, 7, e00078.

Santala, S., Santala, V., Liu, N. & Stephanopoulos, G. (2021) Partitioning metabolism between growth and product synthesis for coordinated production of wax esters in *Acinetobacter baylyi* ADP1. *Biotechnology and Bioengineering*, 118, 2283–2292.

Schindelin, J., Arganda-Carreras, I., Frise, E., Kaynig, V., Longair, M., Pietzsch, T. et al. (2012) Fiji: an open-source platform for biological-image analysis. *Nature Methods*, 9, 676–682.

Si, F., Li, D., Cox, S.E., Sauls, J.T., Azizi, O., Sou, C. et al. (2017) Invariance of initiation mass and predictability of cell size in *Escherichia coli*. *Current Biology*, 27, 1278–1287.

Steigedal, M. & Valla, S. (2008) The Acinetobacter sp. chnB promoter together with its cognate positive regulator ChnR is an attractive new candidate for metabolic engineering applications in bacteria. *Metabolic Engineering*, 10, 121–129.

Stöveken, T., Kalscheuer, R., Malkus, U., Reichelt, R. & Steinbüchel, A. (2005) The wax ester synthase/acyl coenzyme A:Diacylglycerol Acyltransferase from Acinetobacter sp. strain ADP1: characterization of a novel type of acyltransferase. *Journal of Bacteriology*, 187, 1369–1376.

Suárez, G.A., Dugan, K.R., Renda, B.A., Leonard, S.P., Gangavarapu, L.S. & Barrick, J.E. (2020) Rapid and assured genetic engineering methods applied to *Acinetobacter baylyi* ADP1 genome streamlining. *Nucleic Acids Research*, 48, 4585–4600.

Thattai, M. & van Oudenaarden, A. (2001) Intrinsic noise in gene regulatory networks. *Proceedings of the National Academy of Sciences of the United States of America*, 98, 8614–8619.

Tumen-Velasquez, M., Johnson, C.W., Ahmed, A., Dominick, G., Fulk, E.M., Khanna, P. et al. (2018) Accelerating pathway evolution by increasing the gene dosage of chromosomal segments. *Proceedings of the National Academy of Sciences of the United States of America*, 115, 7105–7110.

Volke, D.C. & Nikel, P.I. (2018) Getting bacteria in shape: synthetic morphology approaches for the design of efficient microbial cell factories. *Advanced Biosystems*, 2, 1800111.

Wältermann, M., Hinz, A., Robenek, H., Troyer, D., Reichelt, R., Malkus, U. et al. (2005) Mechanism of lipid-body formation in prokaryotes: how bacteria fatten up. *Molecular Microbiology*, 55, 750–763.

Wang, Y., Wu, H., Jiang, X. & Chen, G.Q. (2014) Engineering Escherichia coli for enhanced production of poly(3-hydroxybutyrate-co-4-hydroxybutyrate) in larger cellular space. *Metabolic Engineering*, 25, 183–193.

Wang, Y., Ling, C., Chen, Y., Jiang, X. & Chen, G.Q. (2019) Microbial engineering for easy downstream processing. *Biotechnology Advances*, 37, 107365.

Wei, L., Zhao, J., Wang, Y., Gao, J., Du, M., Zhang, Y. et al. (2022) Engineering of Corynebacterium glutamicum for high-level γ-aminobutyric acid production from glycerol by dynamic metabolic control. *Metabolic Engineering*, 69, 134–146.

Whinn, K.S., Kaur, G., Lewis, J.S., Schauer, G.D., Mueller, S.H., Jergic, S. et al. (2019) Nuclease dead Cas9 is a programmable roadblock for DNA replication. *Scientific Reports*, 9, 13292.

Woolston, B.M., Emerson, D.F., Currie, D.H. & Stephanopoulos, G. (2018) Rediverting carbon flux in *Clostridium ljungdahlii* using CRISPR interference (CRISPRi). *Metabolic Engineering*, 48, 243–253.

Yenkie, K.M., Wu, W. & Maravelias, C.T. (2017) Synthesis and analysis of separation networks for the recovery of intracellular chemicals generated from microbial-based conversions. *Biotechnology for Biofuels*, 10, 119.

Young, K.D. (2006) The selective value of bacterial shape. *Microbiology and Molecular Biology Reviews*, 70, 660–703.

Zhang, S. & Voigt, C.A. (2018) Engineered dCas9 with reduced toxicity in bacteria: implications for genetic circuit design. *Nucleic Acids Research*, 46, 11115–11125.

Zhang, X., Lin, Y., Wu, Q., Wang, Y. & Chen, G.Q. (2020) Synthetic biology and genome-editing tools for improving PHA metabolic engineering. *Trends in Biotechnology*, 38, 689–700.

Zobel, S., Benedetti, I., Eisenbach, L., de Lorenzo, V., Wierckx, N. & Blank, L.M. (2015) Tn7-based device for calibrated heterologous gene expression in *Pseudomonas putida*. *ACS Synthetic Biology*, 4, 1341–1351.

SUPPORTING INFORMATION

Additional supporting information can be found online in the Supporting Information section at the end of this article.

How to cite this article: Luo, J., Efimova, E., Volke, D.C., Santala, V. & Santala, S. (2022) Engineering cell morphology by CRISPR interference in *Acinetobacter baylyi* ADP1. *Microbial Biotechnology*, 00, 1–19. Available from: https://doi.org/10.1111/1751-7915.14133